ORNL-4810

NATURAL TITANIUM NEUTRON ELASTIC AND INELASTIC SCATTERING CROSS SECTIONS FROM 4.07 TO 8.56 MeV

W. E. Kinney
F. G. Perey

OAK RIDGE NATIONAL LABORATORY
OPERATED BY UNION CARBIDE CORPORATION • FOR THE U.S. ATOMIC ENERGY COMMISSION

Printed in the United States of America. Available from
National Technical Information Service
U.S. Department of Commerce
5285 Port Royal Road, Springfield, Virginia 22151
Price: Printed Copy $4.00; Microfiche $1.45

ORNL-4810
UC-79d

Contract No. W-7405-eng-26

Neutron Physics Division

NATURAL TITANIUM NEUTRON ELASTIC AND INELASTIC SCATTERING CROSS SECTIONS FROM 4.07 TO 8.56 MeV

W. E. Kinney and F. G. Perey

OCTOBER 1973

OAK RIDGE NATIONAL LABORATORY
Oak Ridge, Tennessee 37830
operated by
UNION CARBIDE CORPORATION
for the
U.S. ATOMIC ENERGY COMMISSION

CONTENTS

NATURAL TITANIUM NEUTRON ELASTIC AND INELASTIC SCATTERING CROSS SECTIONS FROM 4.07 TO 8.56 MeV

W. E. Kinney and F. G. Perey

ABSTRACT

Measured cross sections per atom of natural titanium for neutron elastic scattering and for inelastic scattering to levels in ^{48}Ti for incident neutron energies between 4.07 and 8.56 MeV are given and compared with previous results. ENDF/B III MAT 1144 angular distributions are in reasonably good agreement with experimental results at angles less than 40 degrees but differ by as much as an order of magnitude at larger angles. The ENDF/B III MAT 1144 angle-integrated elastic scattering cross sections agree within experimental uncertainties with experimental results at energies below 6.44 MeV but rise 20% above measured values at 8.56 MeV. ENDF/B III MAT 1144 inelastic scattering cross sections to discrete levels in ^{48}Ti are in poor agreement with experimental data because of the predominance of continuum inelastic scattering in ENDF/B III MAT 1144. An evaporation model of inelastic scattering to the continuum is found to be valid for inelastic scattering to levels of excitation energy greater than 6 MeV but is questionable for inelastic scattering to levels of lower excitation energy.

INTRODUCTION

The data reported here are the results of one of a series of experiments to measure neutron elastic and inelastic scattering cross sections at the ORNL Van de Graaffs. Reports in the series are listed in Reference 1. This report presents measured neutron elastic and inelastic scattering cross sections for natural titanium at 11 energies between 4.07 and 8.56 MeV. To assist in the evaluation of the data, the data acquisition and reduction techniques are first briefly discussed. For the purposes of discussion the data are presented in graphical form and are compared with the results of Walt and Beyster[2] and with ENDF/B III (Evaluated Neutron Data File B, Version III) MAT 1144. Tables of numerical values of the elastic scattering cross sections and cross sections for inelastic scattering to discrete levels in the residual nucleus are given in an appendix.

DATA ACQUISITION

The data were obtained with conventional time-of-flight techniques. Pulsed (2 MHz), bunched (approximately 1.5 nsec full width at half maximum, FWHM) deuterons accelerated by the ORNL Van de Graaff's interacted with deuterium in a gas cell to produce neutrons by the D(d,n)^{3}He reaction. The gas cells, of length 1 and 2 cm, were operated at pressures of approximately 1.5 atm and gave neutron energy resolutions of the order of $\pm$60 keV.

The neutrons were scattered from a solid right circular cylindrical sample of natural

titanium, 1.529 cm diameter, 2.621 long of mass 21.49 gm and placed approximately 10 cm from the gas cells when the detector angles were greater than 25 degrees. For smaller detector angles the cell-to-sample distance had to be increased to 33 cm in order to shield the detectors from neutrons coming directly from the gas cells.

The scattered neutrons were detected by 12.5 cm diameter NE-213 liquid scintillators optically coupled to XP-1040 photomultipliers. The scintillators were 2.5 cm thick. Data were taken with three detectors simultaneously. Flight paths were approximately 5 m with the detector angles ranging from 15 to 140 degrees. The gas cell neutron production was monitored by a time-of-flight system which used a 5 cm diameter by 2.5 cm thick NE-213 scintillator viewed by a 56-AVP photomultiplier placed about 4 m from the cell at an angle of 55 degrees with the incident deuteron beam.

For each event a PDP-7 computer was given the flight time of a detected recoil proton event with reference to a beam pulse signal, the pulse height of the recoil proton event, and identification of the detector. The electronic equipment for supplying this information to the computer consisted, for the most part, of standard commercial components. The electronic bias was set at approximately 700 keV neutron energy to ensure good pulse shape discrimination against gamma-rays at all energies.

The detector efficiencies were measured by (n,p) scattering from a 6 mm diameter polyethylene sample and by detecting source $D(d,n)^3He$ neutrons at 0 degrees[3]. Both interactions gave results which agreed with each other and which yielded efficiency versus energy curves that compared well with calculations[4].

DATA REDUCTION

Central to the data reduction process was the use of a light pen with the PDP-7 computer oscilloscope display programs to extract peak areas from spectra. The light pen made a comparatively easy job of estimating errors in the cross section caused by extreme but possible peak shapes.

The reduction process started by normalizing a sample-out to a sample-in time-of-flight spectrum by the ratio of their monitor neutron peak areas, subtracting the sample-out spectrum, and transforming the difference spectrum into a spectrum of center-of-mass cross section versus excitation energy. This transformation allowed ready comparison of spectra taken at different angles and incident neutron energies by removing kinematic effects. It also made all single peaks have approximately the same shape and width regardless of excitation energy (in a time-of-flight spectrum, single peaks broaden with increasing flight time). A spectrum of the variance based on the counting statistics of the initial data was also computed. Figure 1 shows a typical time-of-flight spectrum and its transformed energy spectrum.

The transformed spectra were read into the PDP-7 computer and the peak stripping was done with the aid of the light pen. A peak was stripped by drawing a background beneath it, subtracting the background, and calculating the area, centroid, and FWHM of the difference. The variance spectrum was used to compute a counting statistics variance corresponding to the stripped peak. Peak stripping errors due to uncertainties in the residual background under the peaks or to the tails of imperfectly resolved nearby peaks could be included with the other errors by stripping the peaks several times corresponding to high, low, and best estimates of

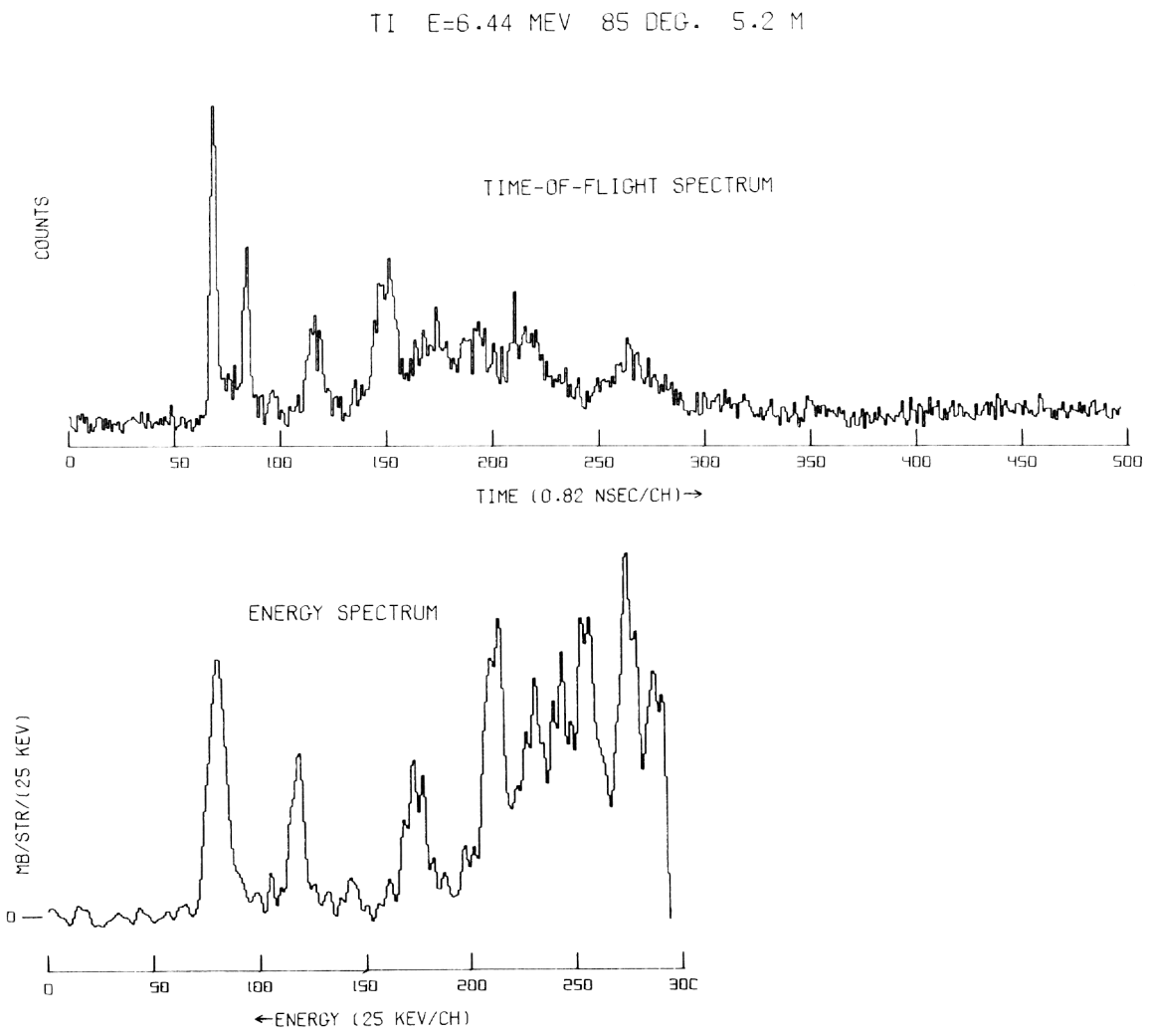

Fig. 1. A typical time-of-flight spectrum for natural titanium with its transformed energy spectrum. The data were taken at 6.44 MeV incident neutron energy at 85 degrees with a 5.2 m flight path. The sample-out spectrum has not been subtracted from the time-of-flight spectrum. Note that the energy spectrum has been offset to allow negative excursions due to statistics in the subtraction of the sample-out. The energy spectrum terminates at approximately 1 MeV scattered neutron energy - very nearly channel 350 in the time-of-flight spectrum.

this background. Although somewhat subjective, the low and high estimates of the cross sections were identified with 95% confidence limits; these, together with the best estimate, defined upper and lower errors due to stripping. When a spectrum was completely stripped, the output information was written on magnetic tape for additional processing by a large computer.

Finite sample corrections were performed according to semianalytic recipes whose constants were obtained from fits to Monte Carlo results[5]. The corrections were as large as 70% in the first minimum of the elastic differential cross section but were typically 10–20% at other angles.

The final error analysis included uncertainties in the geometrical parameters (scatterer size, gas cell-to-scatterer distance, flight paths, etc.) and uncertainties in the finite sample corrections.

The measured differential elastic scattering cross sections were fitted by least squares to a Legendre series:

$$\sigma(\mu = \cos\theta) = \Sigma[(2k+1)/2)]a_k P_k(\mu)$$

the points being weighted by the inverse of their variances which were computed by squaring the average of the upper and lower uncertainties. The common 7% uncertainty in absolute normalization was not included in the variances for the fitting. In order to prevent the fit from giving totally unrealistic values outside the angular range of our measurements, we resorted to the inelegant but workable process of adding three points equally spaced in angle between the largest angle of measurement and 175 degrees. The differential cross sections at the added points were chosen to approximate the diffraction pattern at large angles, but were assigned 50% errors.

RESULTS

Elastic Scattering Differential Cross Sections

Natural titanium contains 5 isotopes from ^{46}Ti through ^{50}Ti. The isotopic abundances[6] are 7.93% ^{46}Ti, 7.28% ^{47}Ti, 73.94% ^{48}Ti, 5.51% ^{49}Ti, and 5.34% ^{50}Ti.

Our differential elastic scattering cross sections for natural titanium are shown in Figure 2 with Legendre fits to the data. Wick's Limit is shown and was used in the fitting. The contribution of inelastic scattering to the 0.160 MeV level in ^{47}Ti, which would not have been resolved from elastic scattering, is negligible.

Figure 3 compares our differential elastic scattering with results of Walt and Beyster (W+B)[2] who measured at 4.1 MeV and with the angular distributions of ENDF/B III MAT 1144, normalized to our angle-integrated data.

At 4.34 MeV, for angles smaller than 35 degrees our two sets of data, obtained with two different experimental arrangements (see section on data acquisition), differ by about 20%, with the lower data in better agreement with that of Walt and Beyster at 4.1 MeV. At angles greater than 50 degrees there are differences with the data of Walt and Beyster, with our data being systematically lower by as much as a factor of two in the first minimum. Resonance structure is still evident in the titanium total cross section at these energies[7] with 4.1 MeV, the energy of the Walt and Beyster measurement, falling in the valley between two small

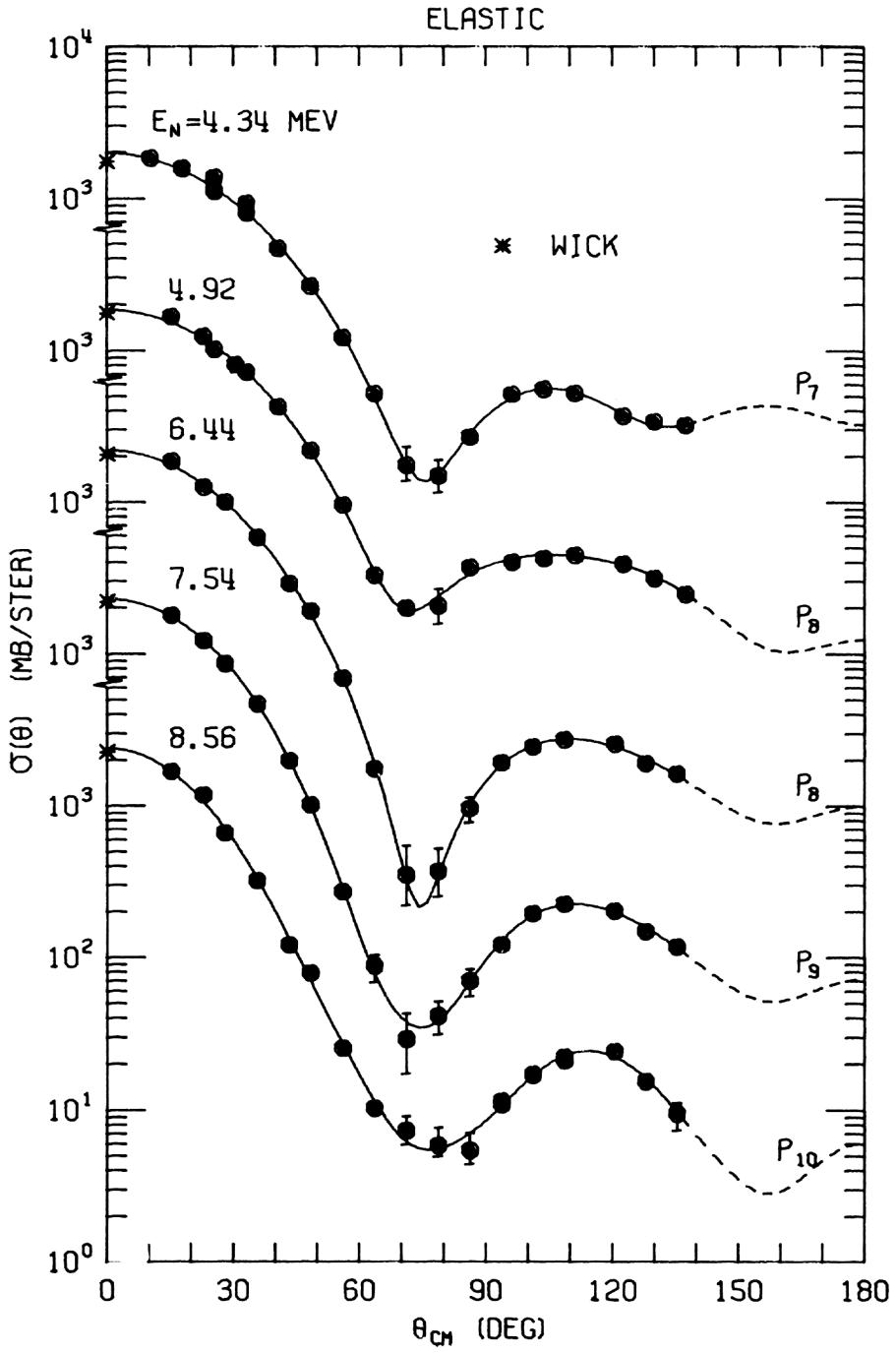

Fig. 2. Our natural titanium neutron differential elastic cross sections with Legendre fits to the data. WICK indicates Wick's Limit which was used in the fitting. The 7% uncertainty in absolute normalization common to all points is not included in the error bars.

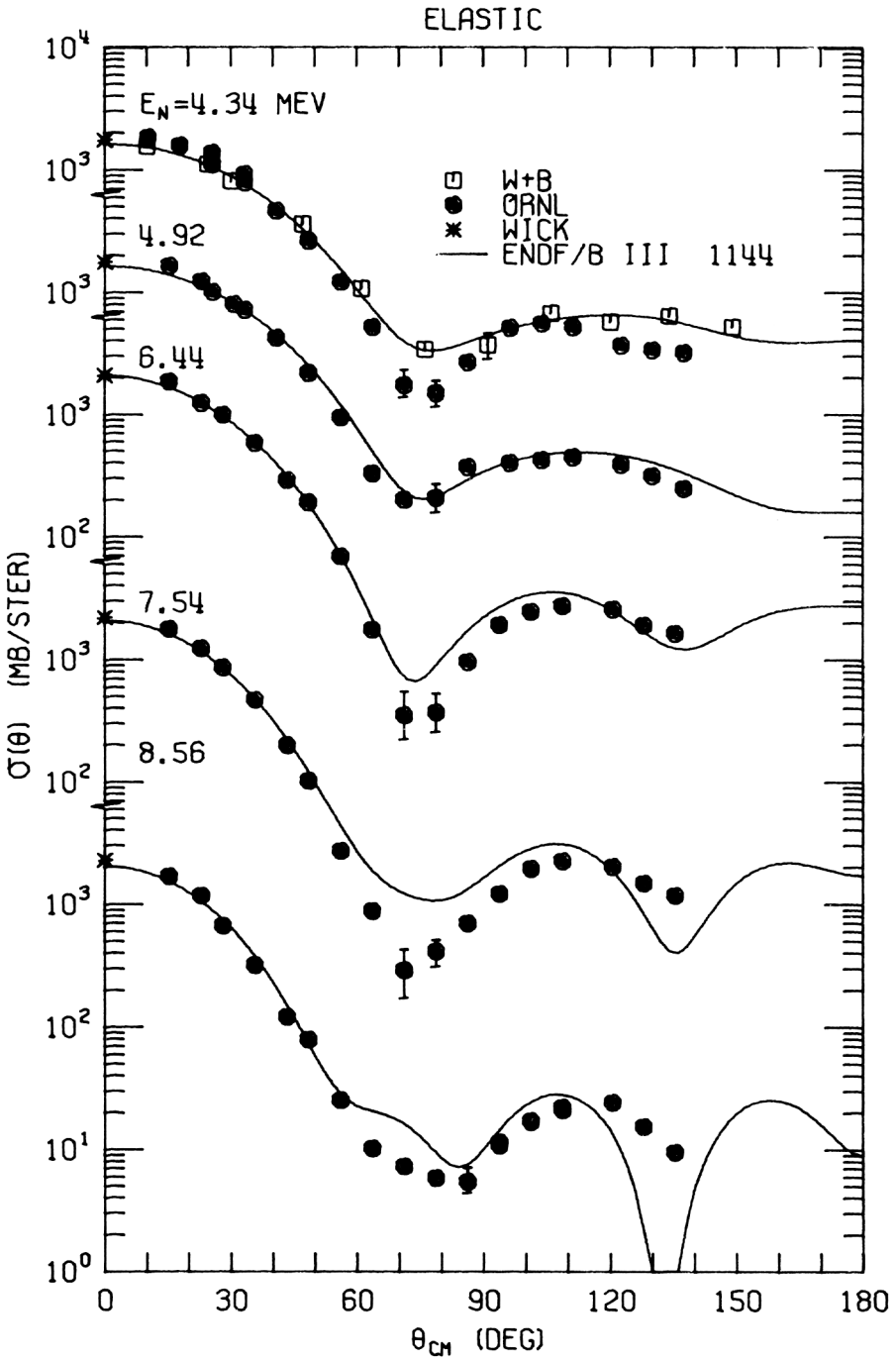

Fig. 3. Our natural titanium neutron differential elastic cross sections compared with the data of Walt and Beyster(W+B) and with the angular distributions of ENDF/B III MAT 1144. WICK indicates Wick's Limit. The 7% uncertainty in absolute normalization common to all points is not included in the error bars.

resonances and 4.34 MeV lying about midway down a resonance at approximately 4.24 MeV. The difference in the energy of the two measurements may account for differences in the differential cross sections.

The ENDF/B III MAT 1144 distributions are in reasonably good agreement with experimental results at angles less than 40 degrees but disagree elsewhere especially in the minima at higher energies: by a factor of 5 in the first minimum at 7.54 MeV and by an order of magnitude in the second minimum at 8.56 MeV. The good agreement of ENDF/B III MAT 1144 with the results of Walt and Beyster is expected since their data was used to generate the ENDF/B III MAT 1144 angular distributions.

Inelastic Scattering Differential Cross Sections

Inelastic scattering to levels in the minor isotopes of natural titanium was too small to extract meaningful cross sections from the data. We have extracted cross sections per atom of natural titanium for inelastic scattering to levels in ^{48}Ti only.

Figure 4 shows our differential cross sections per atom of natural titanium for inelastic scattering to the 0.983 MeV level in ^{48}Ti. This is a 2^+ level and might be expected to show some assymetry due to direct interaction. The angular distributions, however, are nearly symmetric about 90 deg. with the coefficients of the first Legendre Polynomial being less than 13% of the coefficients of the second at all energies(see the appendix).

Figure 5 shows our differential cross sections per atom of natural titanium for inelastic scattering to the combined 2.295 and 2.420 MeV levels in ^{48}Ti. The distributions are isotropic within experimental uncertainties.

Our differential cross sections per atom of natural titanium for inelastic scattering to the 3.224, 3.240, 3.340, 3.360, and 3.380 MeV levels in ^{48}Ti are given in Figure 6. Again, within the experimental uncertainties, the distributions are isotropic.

The small value of the differential cross sections for inelastic scattering to the 3 MeV level in ^{48}Ti prevented their determination at energies greater than 4.34 MeV. The data are shown in Figure 7 along with differential cross sections for inelastic scattering to a group of levels from 3.518 to 3.860 MeV in ^{48}Ti measured at 4.92 MeV. At higher incident neutron energies, scattering to this group of levels is included in the "continuum" discussed below.

ENDF/B III MAT 1144 makes the assumption of isotropic inelastic scattering to all levels.

Excitation Functions

Our angle-integrated differential cross sections per atom of natural titanium are shown as a function of energy in Figure 8. The elastic datum of Walt and Beyster at 4.1 MeV is shown along with the curve from ENDF/B III MAT 1144.

The ENDF/B III MAT 1144 elastic cross sections are in good agreement with experiment below 6.5 MeV but are about 20% higher at 8.56 MeV.

Inelastic scattering cross sections to specific levels decrease with increasing energy as competition from additional exit channels increases.

At incident neutron energies other than 4.34, 4.92, 6.44, 7.54, and 8.56 MeV, data were taken at three angles only. Values of the angle-integrated cross sections for inelastic scattering

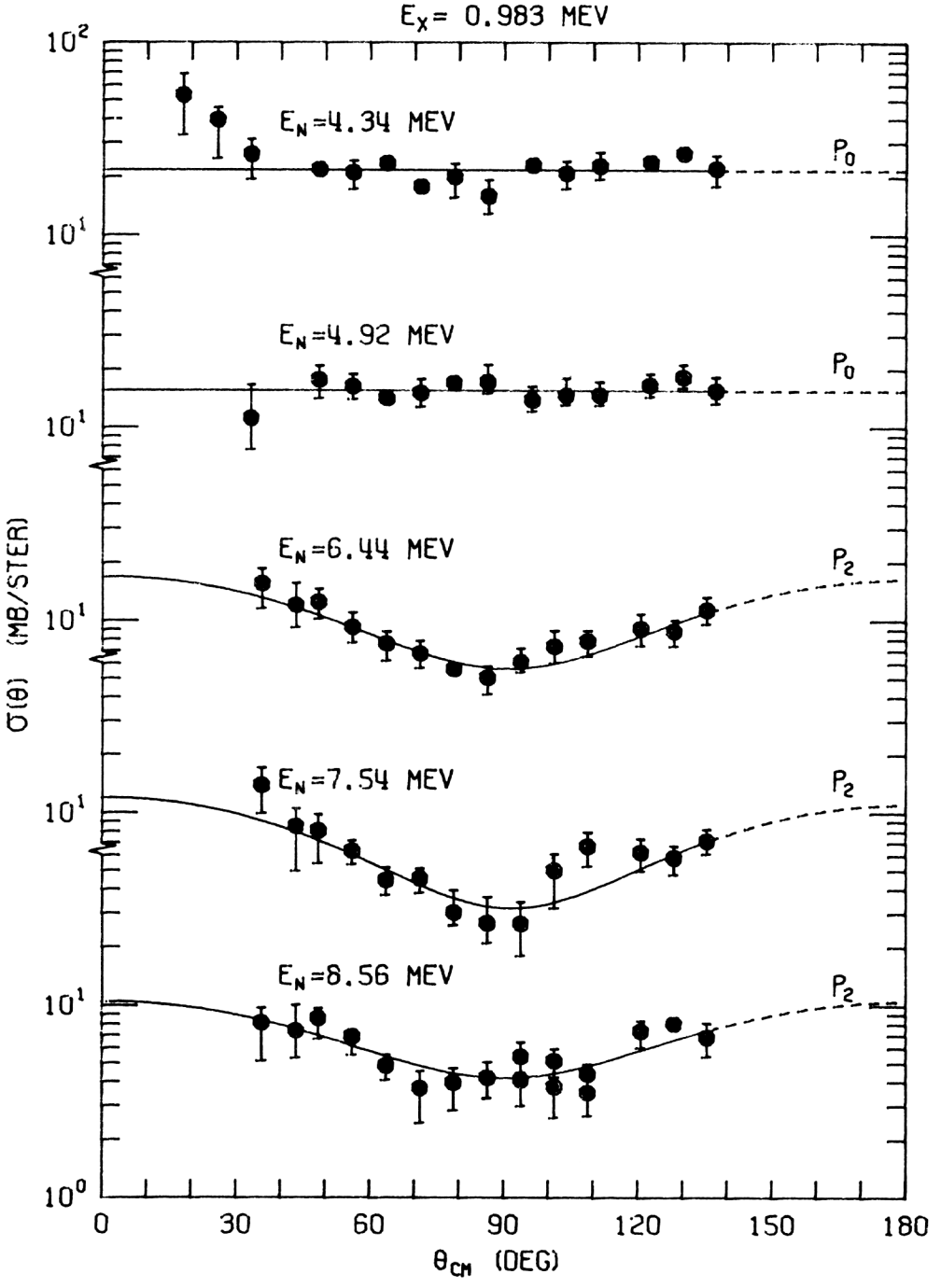

Fig. 4. Our differential cross sections per atom of natural titanium for neutron inelastic scattering to the 0.983 MeV level in ^{48}Ti with Legendre fits to the data.

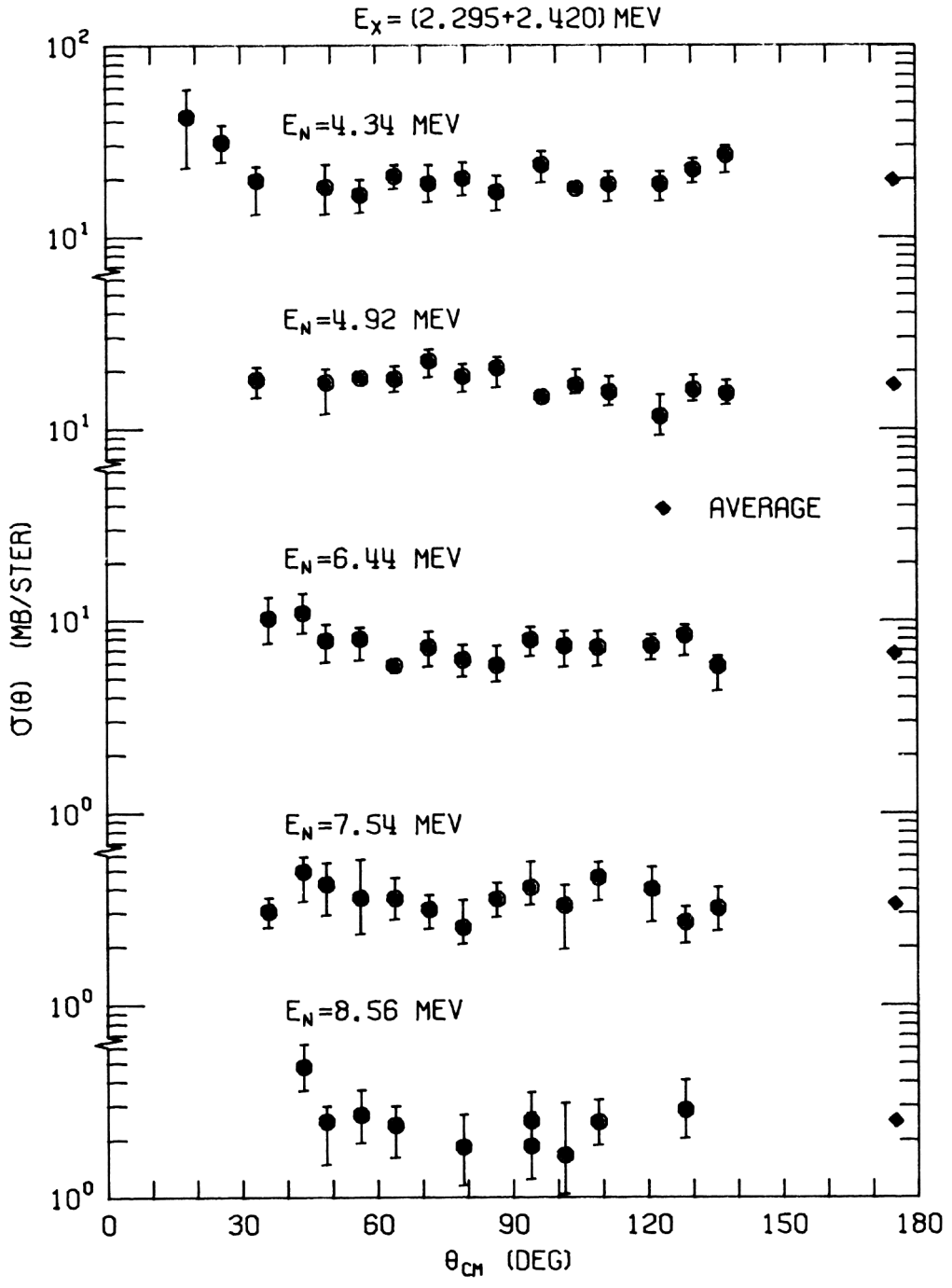

Fig. 5. Our differential cross sections per atom of natural titanium for neutron inelastic scattering to the 2.295 and 2.420 MeV levels in ^{48}Ti.

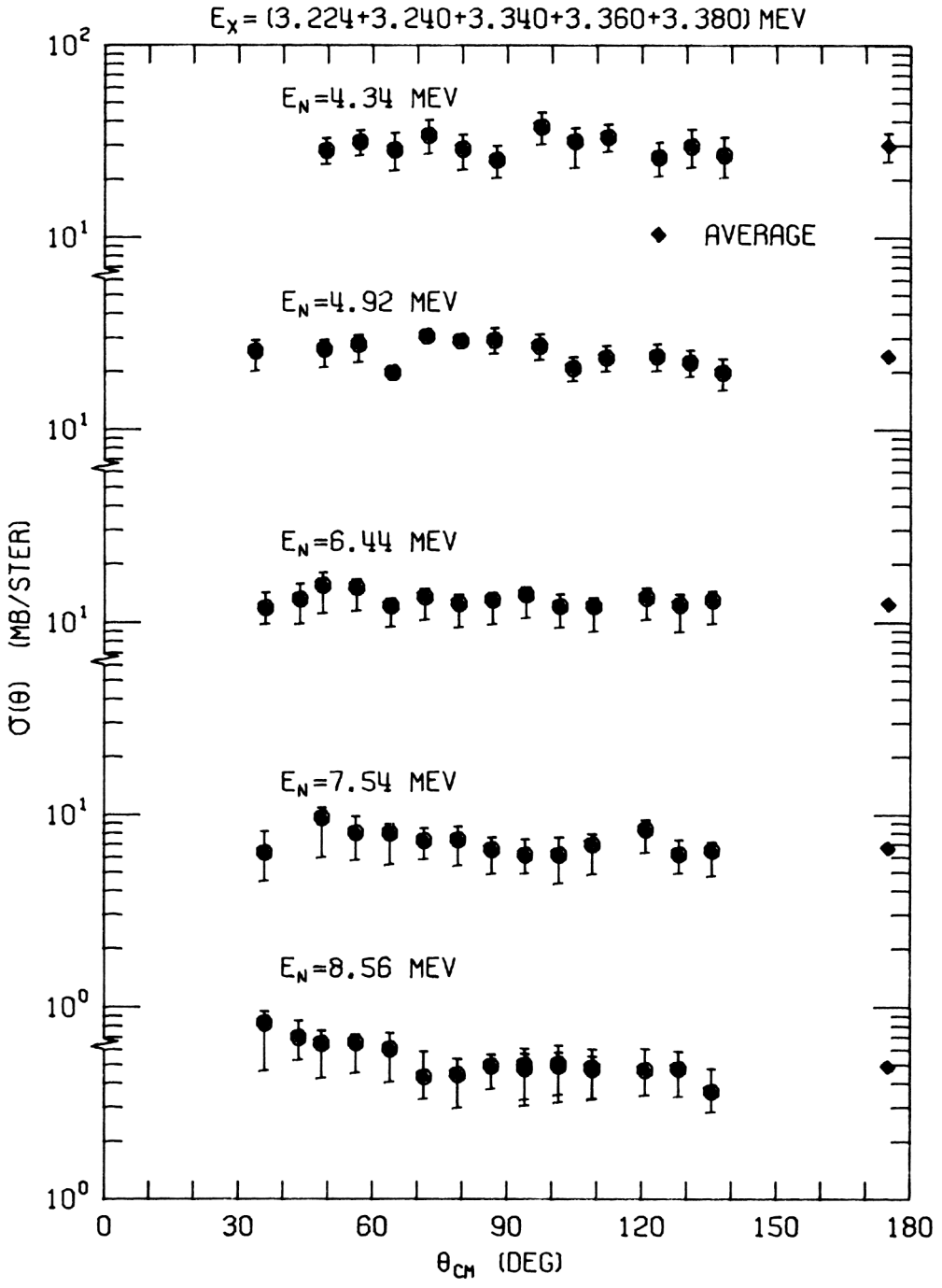

Fig. 6. Our differential cross sections per atom of natural titanium for neutron inelastic scattering to the 3.224 to 3.380 MeV levels in ^{48}Ti.

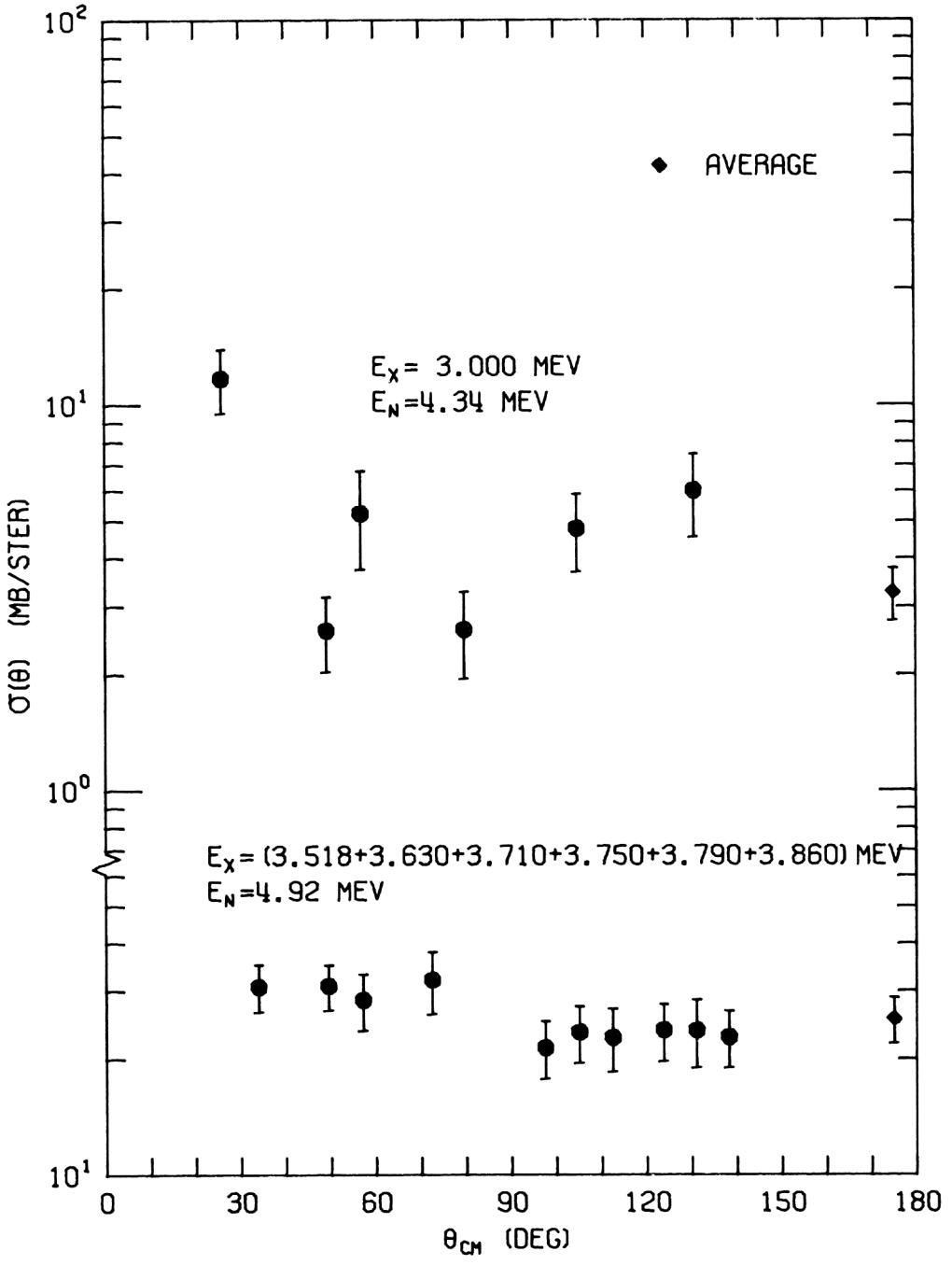

Fig. 7. Our differential cross sections per atom of natural titanium for neutron inelastic scattering to the 3.000 MeV level in ^{48}Ti at an incident neutron energy of 4.34 MeV and to the 3.518 to 3.860 MeV levels in ^{48}Ti at an incident neutron energy of 4.92 MeV.

to the 0.983 MeV level in ^{48}Ti at these energies were corrected for anisotropy by

1) linearly interpolating the normalized Legendre coefficients resulting from the fits to the measured differential cross sections at adjacent energies for which more complete angular distributions were measured, and

2) adjusting the magnitudes of the interpolated Legendre coefficients to give a reasonable fit to the data at the three angles.

The ENDF/B III MAT 1144 cross sections for inelastic scattering to levels indicated by the Q values on the graph are in poor agreement with our data except for the 0.983 MeV level at incident neutron energies less than 5.5 MeV. ENDF/B III MAT 1144, however, accounts for most of its inelastic scattering in this energy region by a continuum with temperatures near 1 MeV. At 4 MeV the continuum accounts for 50% of the inelastic scattering and its contribution rises to 93% at 6 MeV. The ENDF/B III MAT 1144 scattering to discrete levels decreases as the continuum scattering increases.

Inelastic Scattering To The Continuum

At incident neutron energies above 5 MeV we treated inelastic scattering to levels of excitation energy greater than 3.5 MeV as scattering to a continuum of levels rather than attempting to extract cross sections for inelastic scattering to groups of levels or excitation energy intervals. Our "continua" are shown in Figure 9 where angle-averaged differential cross sections for inelastic scattering to an excitation energy versus the excitation energy are shown for incident neutron energies from 6.44 to 8.56 MeV. Some levels or groups of levels are clearly preferentially excited giving rise to peaks in the cross sections at excitation energies of approximately 3.75, 4.1, 4.4, 4.9, 5.6, 5.9, and possibly 6.1 MeV.

The success one might expect from applying an evaporation model to our "continua" may be judged from Figure 10 where SIG(E $\rightarrow$ E')/E' versus E' is plotted as a function of E' where SIG(E $\rightarrow$ E') = angle-averaged differential cross section for scattering from incident energy E to exit energy dE' about E'.

The lines are least squares fits to the data but over a limited energy range: to E' = 1.5 MeV for E = 7.54 MeV, to E' = 2.0 MeV for E = 8.04 MeV, and to E' = 2.5 MeV for E = 8.56 MeV. The temperatures resulting from the fits are indicated with the errors being the fitting errors only. The ENDF/B III MAT 1144 temperatures describing inelastic scattering to the continuum vary linearly from a value of 0.95 MeV at an incident energy of 1.75 MeV to a value of 1.18 MeV at an incident energy of 10 MeV.

An evaporation model appears to be a reasonable representation of our data above an excitation energy of 6 MeV in the residual nucleus but at lower excitation energies the data vary by a factor of two both above and below values given by an evaporation spectrum.

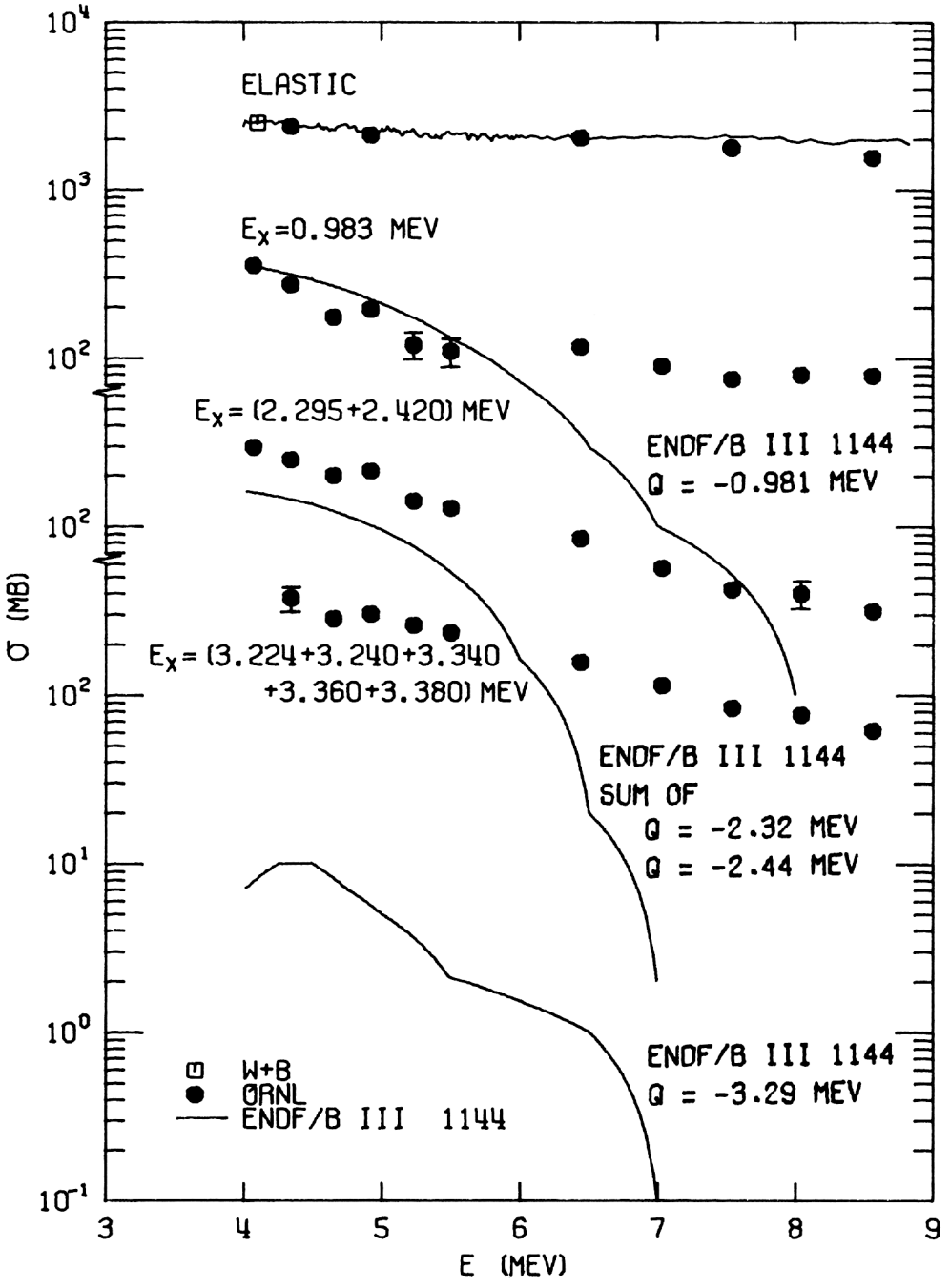

Fig. 8. Our angle-integrated cross sections for neutron elastic scattering on natural titanium and cross sections per atom of natural titanium for inelastic scattering to levels in ^{48}Ti as a function of incident neutron energy. The datum of Walt and Beyster(W+B) is included. The curves are cross sections from ENDF/B III MAT 1144.

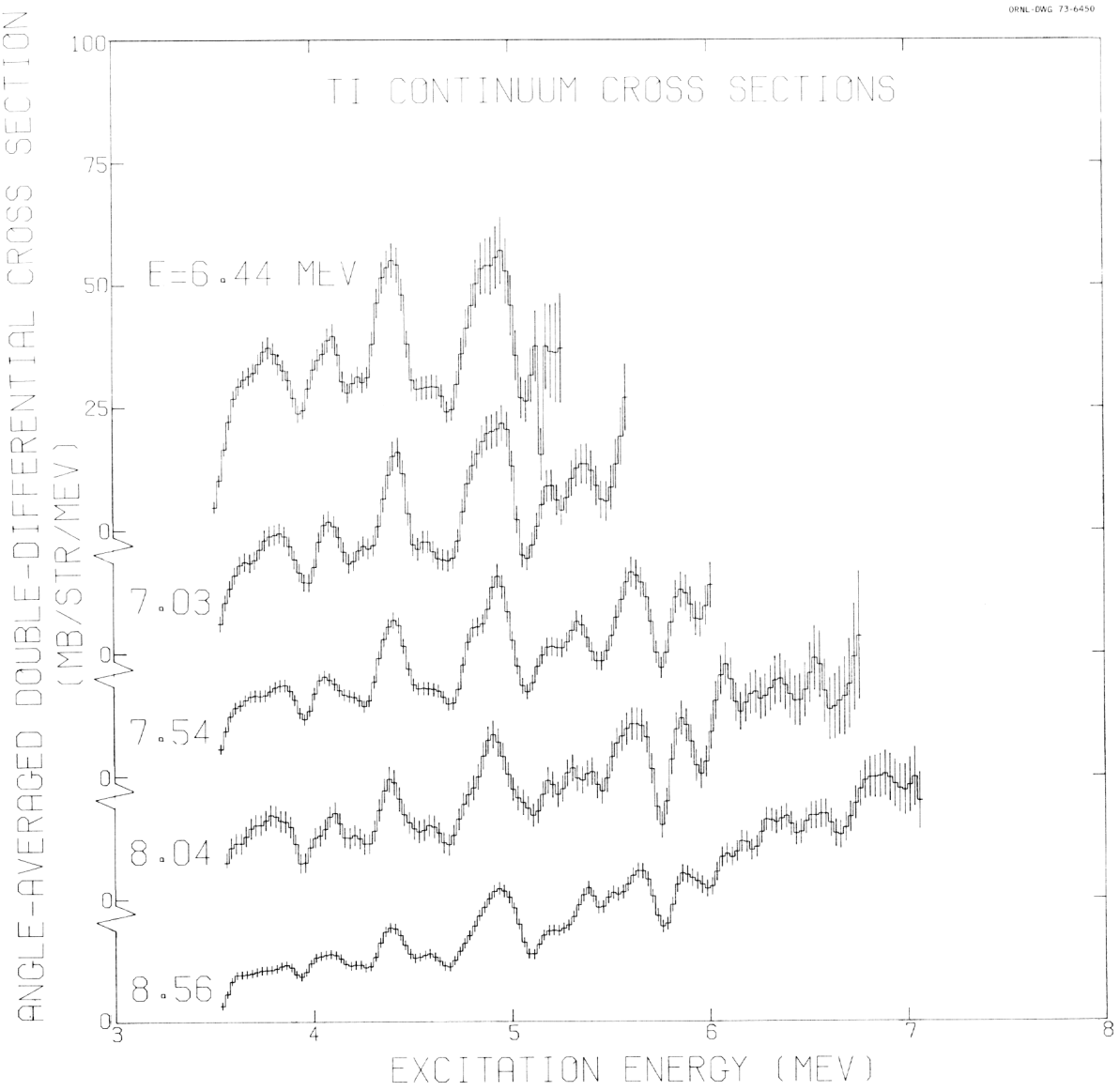

Fig. 9. Natural titanium angle-averaged cross sections for inelastic scattering to the "continuum" as a function of excitation energy for incident neutron energies, E, from 6.44 to 8.56 MeV.

ORNL-DWG 73-6448

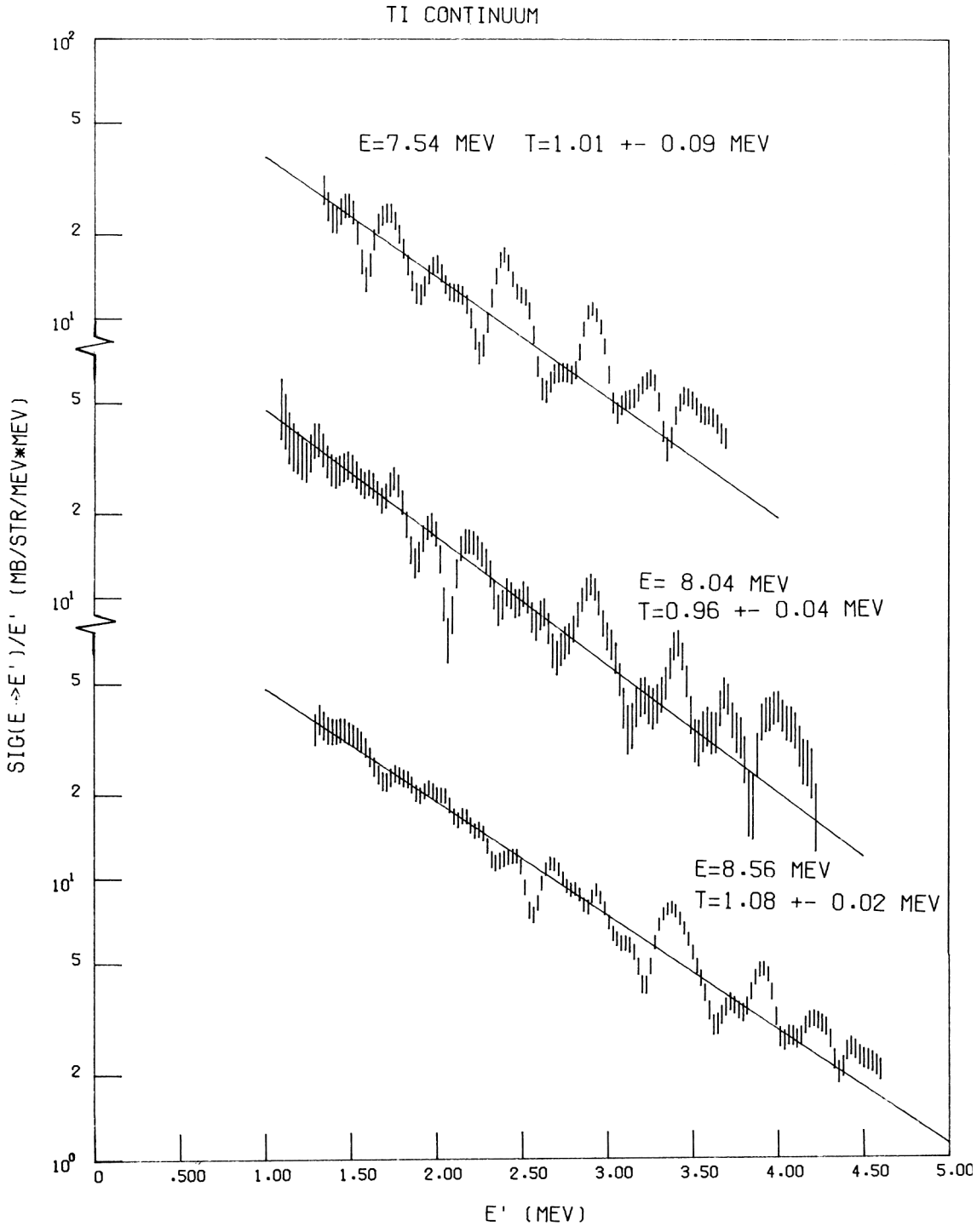

Fig. 10. Natural titanium angle-averaged cross sections for inelastic scattering to the continuum divided by the out-going neutron energy as a function of out-going neutron energy for incident neutron energies, E, from 7.54 to 8.56 MeV. Least squares fits are shown with the resulting temperatures, T. The fits were made only below $E' = 3$ MeV at $E = 8.56$ MeV; $E' = 2.5$ MeV at $E = 8.04$ MeV; and $E' = 2$ MeV at $E = 7.54$ MeV.

CONCLUSIONS

The differences of 20% to 50% between our differential elastic scattering cross sections at 4.34 MeV and those of Walt and Beyster[2] at 4.1 MeV may be accounted for by the resonance structure still evident in the titanium total cross section at these energies. ENDF/B III MAT 1144 elastic angular distributions are in reasonably good agreement with our data at angles less than 40 degrees but differ by as much as an order of magnitude at larger angles. ENDF/B III MAT 1144 angle-integrated elastic scattering cross sections agree with experimental results within experimental uncertainties up to 6.44 MeV but rise above experiment at higher energies, being 20% higher at 8.56 MeV. ENDF/B III MAT 1144 inelastic scattering to discrete levels agrees very poorly with our results because of the strong dependance it places on an evaporation model of inelastic scattering to a continuum. Our data show an evaporation model to be a reasonable description of inelastic scattering to levels of excitation energy above 6 MeV but to be of questionable validity for inelastic scattering to levels of lower excitation energy.

ACKNOWLEDGMENTS

Many have contributed to this experimental program at one time or another and we would like to thank them for their contributions. In particular, we would like to acknowledge the help of J. K. Dickens, J. W. McConnell, J. A. Biggerstaff, A. M. Marusak, P. H. Stelson, C. O. LeRigoleur, and E. Hungerford.

We are deeply indebted to F. C. Maienschein, director of the Neutron Physics Division, for his support of the experiment with the use of computers in report preparation and type setting which produced this report and the other six of our last seven reports.

REFERENCES

1. F. G. Perey and W. E. Kinney, "Carbon Neutron Elastic- and Inelastic- Scattering Cross Sections from 4.5 to 8.5 MeV", ORNL–4441 (December 1970).

F. G. Perey, C. O. LeRigoleur and W. E. Kinney, "Nickel–60 Neutron Elastic- and Inelastic-Scattering Cross Sections from 6.5 to 8.5 MeV", ORNL–4523 (April 1970).

W. E. Kinney and F. G. Perey, Neutron Elastic- and Inelastic-Scattering Cross Sections from ^{56}Fe in the Energy Range 4.19 to 8.56 MeV", ORNL–4515 (June 1970).

F. G. Perey and W. E. Kinney, Calcium Neutron Elastic- and Inelastic- Scattering Cross Sections from 4.0 to 8.5 MeV", ORNL–4519 (April 1970).

F. G. Perey and W. E. Kinney, "Sulfur Neutron Elastic- and Inelastic- Scattering Cross Sections from 4 to 8.5 MeV", ORNL–4539 (June 1970).

W. E. Kinney and F. G. Perey, "Neutron Elastic- and Inelastic- Scattering Cross Sections for Co in the Energy Range 4.19 to 8.56 MeV", ORNL–4549 (June 1970).

W. E. Kinney and F. G. Perey, "Neutron Elastic- and Inelastic- Scattering Cross Sections for Mg in the Energy Range 4.19 to 8.56 MeV", ORNL–4550 (June 1970).

W. E. Kinney and F. G. Perey, "Neutron Elastic- and Inelastic- Scattering Cross Sections for Si in the Energy Range 4.19 to 8.56 MeV", ORNL–4517 (July 1970).

F. G. Perey and W. E. Kinney, "Neutron Elastic and Inelastic– Scattering Cross Sections for Na in the Energy Range of 5.4 to 8.5 MeV", ORNL–4518 (August 1970).

W. E. Kinney and F. G. Perey, "Al Neutron Elastic- and Inelastic- Scattering Cross Sections from 4.19 to 8.56 MeV", ORNL–4516 (October 1970).

F. G. Perey and W. E. Kinney, "V Neutron Elastic- and Inelastic- Scattering Cross Sections from 4.19 to 8.56 MeV", ORNL–4551 (October 1970).

F. G. Perey and W. E. Kinney, "Neutron Elastic- and Inelastic- Scattering Cross Sections for Yttrium in the Energy Range 4.19 to 8.56 MeV", ORNL–4552 (December 1970).

W. E. Kinney and F. G. Perey, "Neutron Elastic- and Inelastic- Scattering Cross Sections for Oxygen in the Energy Range 4.34 to 8.56 MeV", ORNL–4780 (April 1972).

W. E. Kinney and F. G. Perey, "W Neutron Elastic- and Inelastic– Scattering Cross Sections from 4.34 to 8.56 MeV", ORNL–4803 (May 1973).

W. E. Kinney and F. G. Perey, "Natural Nickel and ^{60}Ni Neutron Elastic and Inelastic Scattering Cross Sections from 4.07 to 8.56 MeV", ORNL–4807 (October 1973).

W. E. Kinney and F. G. Perey, "Natural Chromium and ^{52}Cr Neutron Elastic and Inelastic Scattering Cross Sections from 4.07 to 8.56 MeV", ORNL–4806 (October 1973).

F. G. Perey and W. E. Kinney, "Nitrogen Neutron Elastic and Inelastic Scattering Cross Sections from 4.34 to 8.56 MeV", ORNL–4805 (October 1973).

W. E. Kinney and F. G. Perey, "^{54}Fe Neutron Elastic and Inelastic Scattering Cross Sections from 4.34 to 8.56 MeV", ORNL–4907 (October 1973).

W. E. Kinney and F. G. Perey "^{63}Cu and ^{65}Cu Neutron Elastic and Inelastic Scattering Cross Sections from 5.50 to 8.50 MeV", ORNL–4908 (October 1973).

W. E. Kinney and F. G. Perey, "^{206}Pb, ^{207}Pb, and ^{208}Pb Neutron Elastic and Inelastic Scattering Cross Sections from 5.50 to 8.50 MeV", ORNL–4909 (October 1973)

2. M. Walt and J. R. Beyster, Phys. Rev. *98*, 677 (1955).

3. W. E. Kinney, "Neutron Elastic and Inelastic Scattering from ^{56}Fe from 4.60 to 7.55 MeV", ORNL-TM–2052 (January 1968).

4. R. E. Textor and V. V. Verbinski, "05S: A Monte Carlo Code for Calculating Pulse Height Distributions Due to Monoenergetic Neutrons Incident on Organic Scintillators", ORNL–4160 (February 1968).

5. W. E. Kinney, Nucl. Instr. and Methods *83*, 15 (1970).

6. C. Michael Lederer, Jack M. Hollander, and Isadore Perlman, "Table of Isotopes" Sixth Edition, John Wiley & Sons, Inc. (1967).

7. M. D. Goldberg, *et al.*, BNL–325, Supp. 2 (February 1966).

APPENDIX

Tabulated Values of Natural Titanium Neutron Elastic Scattering Cross Sections and Cross Sections for Inelastic Scattering To Discrete Levels

Our measured values for natural titanium neutron elastic scattering and cross sections for inelastic scattering to discrete levels are tabulated below. The uncertainties in differential cross sections ,indicated by $\triangle$ in the tables, are relative and do *not* include a $\pm 7\%$ uncertainty in detector efficiency which is common to all points. The $\pm 7\%$ uncertainty is included in the integrated and average values. The total cross sections, σ_t, are those we used in the computation of Wick's Limit and were not measured by us.

We have not included the cross sections for inelastic scattering to the continuum. They are available from the National Neutron Cross Section Center, Brookhaven National Laboratory, or from us.

$E_n = 4.07 \pm 0.08$ MeV
(n,n′) to: 0.983 MeV Level

θ_{cm}	$d\sigma/d\omega$	△ (%)	
deg.	mb/str	+	−
71.30	27.14	13.6	11.5
78.86	31.64	9.1	12.3
86.38	26.67	9.9	12.9

$\int(d\sigma/d\omega)d\omega = 355.02\,\text{mb} \pm 9.5\,\%$

Legendre Fit, Order = 0

k	a_k	△(%)
0	56.50330	6.5

$E_n = 4.07 \pm 0.08$ MeV
(n,n′) to: 2.295 MeV Level
+ 2.420 MeV Level

θ_{cm}	$d\sigma/d\omega$	△ (%)	
deg.	mb/str	+	−
71.84	19.81	37.6	21.8
79.39	28.10	8.7	20.4
86.92	23.17	11.4	19.6

Avg. $d\sigma/d\omega = 23.57\,\text{mb/str} \pm 12.6\,\%$
$\int(d\sigma/d\omega)d\omega = 296.23\,\text{mb} \pm 12.6\,\%$

$E_n = 4.07 \pm 0.08$ MeV
(n,n′) to: 3.000 MeV Level

θ_{cm}	$d\sigma/d\omega$	△ (%)	
deg.	mb/str	+	−
79.89	4.11	47.3	37.4
87.43	6.52	26.4	34.0

Avg. $d\sigma/d\omega = 5.20\,\text{mb/str} \pm 30.2\,\%$
$\int(d\sigma/d\omega)d\omega = 65.29\,\text{mb} \pm 30.2\,\%$

$E_n = 4.34 \pm 0.07$ MeV
Elastic Scattering

θ_{cm}	$d\sigma/d\omega$	△ (%)	
deg.	mb/str	+	−
10.21	1837.69	5.2	6.0
17.87	1589.22	6.3	6.9
17.87	1564.69	5.3	8.5
25.51	1116.75	5.9	7.7
25.51	1373.51	5.5	9.6
25.51	1102.65	4.5	5.2
33.15	789.86	4.8	8.1
33.15	925.18	6.1	7.2
40.77	463.78	6.0	6.7
48.39	263.40	5.9	5.9
55.99	121.25	8.8	7.5
63.57	51.84	11.5	11.9
71.13	17.35	32.1	21.0
78.67	14.86	26.1	22.6
86.20	26.80	17.7	14.3
96.20	51.34	10.9	8.7
103.67	55.68	11.0	14.5
111.13	51.95	10.4	10.2
122.53	36.81	13.0	12.1
129.94	33.73	20.8	11.6
137.33	31.87	14.1	12.0

$\int(d\sigma/d\omega)d\omega = 2383.78\text{mb} \pm 7.2\,\%$
Wick's Limit = $1742.37\text{mb} \pm 8.1\,\%$
$\sigma_T = 3.70\text{b} \pm 2.0\,\%$

Legendre Fit, Order = 7

k	a_k	△(%)
0	379.39111	1.7
1	261.56030	2.1
2	196.99940	2.3
3	126.40178	2.8
4	62.31763	4.7
5	19.63194	12.0
6	5.90720	28.6
7	3.49833	38.3

$E_n = 4.34 \pm 0.07$ MeV
(n,n′) to: 0.983 MeV Level

θ_{cm} deg.	$d\sigma/d\omega$ mb/str	△ (%) +	−
17.92	53.48	28.7	38.3
25.58	39.69	15.6	37.2
33.24	26.19	19.5	25.8
48.51	21.79	12.9	13.4
56.13	21.02	15.5	17.7
63.72	23.48	13.8	13.4
71.29	17.77	14.4	11.1
78.83	19.95	17.6	21.7
86.36	15.84	21.6	18.5
96.36	23.07	10.7	15.2
103.84	20.85	15.7	16.5
111.29	22.76	18.3	14.4
122.67	23.73	10.5	10.0
130.07	26.46	14.5	12.6
137.44	22.03	17.8	18.7

$\int(d\sigma/d\omega)d\omega = 272.30\,\text{mb} \pm 8.1\ \%$

Legendre Fit, Order = 0

k	a_k	△(%)
0	43.33794	4.0

$E_n = 4.34 \pm 0.07$ MeV
(n,n′) to: 2.295 MeV Level
+ 2.420 MeV Level

θ_{cm} deg.	$d\sigma/d\omega$ mb/str	△ (%) +	−
18.05	42.12	40.4	45.5
25.77	31.08	22.6	21.5
33.48	19.56	18.2	33.3
48.85	18.10	31.3	27.6
56.48	16.47	20.0	19.3
64.11	20.72	14.3	14.5
71.71	18.88	25.4	19.9
79.26	20.17	21.1	18.9
86.80	17.12	21.0	20.0
96.81	23.82	16.9	19.6
104.27	17.81	15.2	12.5
111.68	18.69	17.0	18.5
123.06	18.83	16.0	18.7
130.41	22.49	14.0	15.6
137.74	26.69	11.7	19.4

Avg. $d\sigma/d\omega = 19.78\text{mb/str} \pm 10.4\%$
$\int(d\sigma/d\omega)d\omega = 248.58\text{mb} \pm 10.4\%$

$E_n = 4.34 \pm 0.07$ MeV
(n,n′) to: 3.000 MeV Level

θ_{cm} deg.	$d\sigma/d\omega$ mb/str	△ (%) +	−
25.91	11.70	18.8	18.8
49.12	2.60	21.9	21.9
56.82	5.24	28.7	28.7
79.70	2.61	25.3	25.3
104.67	4.78	22.8	22.8
130.74	5.99	24.3	24.3

Avg. $d\sigma/d\omega = 3.26\text{mb/str} \pm 15.6\%$
$\int(d\sigma/d\omega)d\omega = 40.95\text{mb} \pm 15.6\%$

Data at the Following Angles
Excluded from the Average:
25.91

$E_n = 4.34 \pm 0.07$ MeV
(n,n') to: 3.224 MeV Level
+ 3.240 MeV Level
+ 3.340 MeV Level
+ 3.360 MeV Level
+ 3.380 MeV Level

θ_{cm}	$d\sigma/d\omega$	Δ (%)	
deg.	mb/str	+	−
49.46	28.40	15.4	15.4
57.07	31.39	14.8	14.8
64.80	28.57	22.0	22.0
72.42	34.02	19.7	19.7
80.02	28.81	18.3	21.6
87.56	25.15	18.9	18.9
97.59	37.60	18.7	18.7
105.01	31.55	17.1	26.9
112.43	33.18	16.0	16.0
123.69	25.99	19.8	19.8
131.02	29.75	22.1	22.1
138.26	26.76	23.3	23.3

Avg. $d\sigma/d\omega$ = 29.82 mb/str ± 16.6 %
$\int(d\sigma/d\omega)d\omega$ = 374.66 mb ± 16.6 %

$E_n = 4.65 \pm 0.07$ MeV
(n,n') to: 0.983 MeV Level

θ_{cm}	$d\sigma/d\omega$	Δ (%)	
deg.	mb/str	+	−
71.27	15.12	23.3	19.1
78.82	14.65	19.6	12.5
86.35	13.08	19.2	11.3

$\int(d\sigma/d\omega)d\omega$ = 174.53 mb ± 11.6 %

Legendre Fit, Order = 0

k	a_k	Δ(%)
0	27.77669	9.3

$E_n = 4.65 \pm 0.07$ MeV
(n,n') to: 2.295 MeV Level

θ_{cm}	$d\sigma/d\omega$	Δ (%)	
deg.	mb/str	+	−
71.60	6.97	20.7	19.7
79.17	8.24	21.4	21.4

Avg. $d\sigma/d\omega$ = 7.48 mb/str ± 16.9 %
$\int(d\sigma/d\omega)d\omega$ = 94.02 mb ± 16.9 %

$E_n = 4.65 \pm 0.07$ MeV
(n,n') to: 2.295 MeV Level
+ 2.420 MeV Level

θ_{cm}	$d\sigma/d\omega$	Δ (%)	
deg.	mb/str	+	−
71.63	17.12	8.0	8.0
79.19	15.39	7.4	7.4
86.73	15.39	14.2	12.7

Avg. $d\sigma/d\omega$ = 15.97 mb/str ± 9.6 %
$\int(d\sigma/d\omega)d\omega$ = 200.64 mb ± 9.6 %

$E_n = 4.65 \pm 0.07$ MeV
(n,n') to: 2.295 MeV Level
+ 2.420 MeV Level
+ 3.000 MeV Level

θ_{cm}	$d\sigma/d\omega$	Δ (%)	
deg.	mb/str	+	−
71.63	16.44	17.1	17.1
79.19	16.29	15.3	15.3

Avg. $d\sigma/d\omega$ = 16.36 mb/str ± 13.9 %
$\int(d\sigma/d\omega)d\omega$ = 205.54 mb ± 13.9 %

$E_n = 4.65 \pm 0.07$ MeV
(n,n') to: 2.420 MeV Level

θ_{cm} deg.	$d\sigma/d\omega$ mb/str	△ (%) +	−
71.65	9.30	16.0	21.9
79.22	8.49	34.0	34.0

Avg. $d\sigma/d\omega$ = 9.04 mb/str ± 20.1 %
$\int(d\sigma/d\omega)d\omega$ = 113.63 mb ± 20.1 %

$E_n = 4.65 \pm 0.07$ MeV
(n,n') to: 3.224 MeV Level
+ 3.240 MeV Level

θ_{cm} deg.	$d\sigma/d\omega$ mb/str	△ (%) +	−
72.08	11.41	17.6	17.6
79.67	9.58	21.5	21.5

Avg. $d\sigma/d\omega$ = 10.54 mb/str ± 16.2 %
$\int(d\sigma/d\omega)d\omega$ = 132.42 mb ± 16.2 %

$E_n = 4.65 \pm 0.07$ MeV
(n,n') to: 3.224 MeV Level
+ 3.240 MeV Level
+ 3.340 MeV Level
+ 3.360 MeV Level
+ 3.380 MeV Level

θ_{cm} deg.	$d\sigma/d\omega$ mb/str	△ (%) +	−
72.15	26.69	11.3	12.1
79.73	20.94	13.8	14.6
87.28	20.73	13.8	12.2

Avg. $d\sigma/d\omega$ = 22.65 mb/str ± 12.1 %
$\int(d\sigma/d\omega)d\omega$ = 284.68 mb ± 12.1 %

$E_n = 4.65 \pm 0.07$ MeV
(n,n') to: 3.340 MeV Level
+ 3.360 MeV Level
+ 3.380 MeV Level

θ_{cm} deg.	$d\sigma/d\omega$ mb/str	△ (%) +	−
72.21	13.27	17.7	17.7
79.78	10.83	26.1	26.1

Avg. $d\sigma/d\omega$ = 12.35 mb/str ± 17.1 %
$\int(d\sigma/d\omega)d\omega$ = 155.23 mb ± 17.1 %

$E_n = 4.92 \pm 0.06$ MeV
Elastic Scattering

θ_{cm} deg.	$d\sigma/d\omega$ mb/str	△ (%) +	−
15.32	1660.58	5.3	6.3
22.97	1240.45	6.5	9.3
25.51	1011.31	4.4	4.8
30.61	803.62	5.4	7.4
33.15	718.29	5.6	8.7
40.78	423.09	5.0	5.0
48.39	218.44	5.4	4.7
55.99	94.83	10.0	8.7
63.57	32.75	8.9	10.4
71.13	19.89	14.5	16.8
78.67	20.63	29.0	24.0
86.20	37.06	11.2	15.2
96.20	40.19	13.0	12.1
103.67	42.38	14.6	11.3
111.13	44.64	8.7	6.9
122.53	38.85	12.6	9.1
129.94	31.24	14.7	16.8
137.33	24.66	18.8	11.7

$\int(d\sigma/d\omega)d\omega = 2110.15\,\text{mb} \pm 7.3\,\%$
Wick's Limit $= 1767.45\,\text{mb} \pm 8.1\,\%$
$\sigma_T = 3.50\,\text{b} \pm 2.0\,\%$

Legendre Fit, Order = 8

k	a_k	△(%)
0	335.84106	1.9
1	240.29784	2.4
2	176.27179	2.7
3	120.88876	3.3
4	60.44460	5.4
5	22.14236	11.9
6	6.15647	32.5
7	0.64561	225.6
8	0.22076	432.2

$E_n = 4.92 \pm 0.06$ MeV
(n,n′) to: 0.983 MeV Level

θ_{cm} deg.	$d\sigma/d\omega$ mb/str	△ (%) +	−
33.23	11.14	49.9	31.1
48.49	17.71	18.4	20.3
56.10	16.30	16.1	14.0
63.69	14.17	11.4	12.5
71.27	15.11	18.0	15.3
78.81	17.00	13.1	12.3
86.34	17.21	23.3	12.3
96.34	13.86	17.8	12.4
103.81	14.64	23.5	10.7
111.26	14.67	18.0	11.1
122.64	16.61	14.8	13.0
130.05	18.23	16.5	12.1
137.43	15.48	18.4	13.9

$\int(d\sigma/d\omega)d\omega = 194.77\text{mb} \pm 8.2\,\%$

Legendre Fit, Order = 0

k	a_k	△(%)
0	30.99889	4.3

$E_n = 4.92 \pm 0.06$ MeV
(n,n′) to: 2.295 MeV Level
+ 2.420 MeV Level

θ_{cm} deg.	$d\sigma/d\omega$ mb/str	△ (%) +	−
33.41	17.93	16.0	19.1
48.75	17.37	17.2	30.8
56.38	18.37	14.6	10.4
64.00	18.15	16.6	14.2
71.59	22.53	14.8	17.9
79.14	18.79	15.8	17.0
86.68	20.77	13.4	21.0
96.68	14.69	15.2	12.0
104.16	16.88	20.3	9.7
111.58	15.44	20.7	14.7
122.94	11.61	29.0	20.4
130.32	15.94	19.3	12.9
137.66	15.26	16.8	12.5

Avg. $d\sigma/d\omega = 16.96\text{mb/str} \pm 9.8\,\%$
$\int(d\sigma/d\omega)d\omega = 213.06\text{mb} \pm 9.8\,\%$

$E_n = 4.92 \pm 0.06$ MeV
(n,n′) to: 3.224 MeV Level
+ 3.240 MeV Level
+ 3.340 MeV Level
+ 3.360 MeV Level
+ 3.380 MeV Level

θ_{cm}	$d\sigma/d\omega$	Δ (%)	
deg.	mb/str	+	−
33.66	25.62	13.9	21.1
49.08	26.16	12.2	19.3
56.76	27.82	11.6	19.1
64.40	19.76	13.4	13.9
72.03	30.65	13.4	13.4
79.61	28.92	12.4	12.4
87.13	29.30	15.3	15.3
97.16	27.19	15.4	15.4
104.61	20.88	14.2	14.2
112.03	23.65	15.3	15.3
123.34	24.03	15.9	15.9
130.67	22.36	15.7	15.7
137.97	19.73	18.4	18.4

Avg. $d\sigma/d\omega$ = 24.08 mb/str ± 10.5 %
$\int(d\sigma/d\omega)d\omega$ = 302.57 mb ± 10.5 %

$E_n = 4.92 \pm 0.06$ MeV
(n,n′) to: 3.518 MeV Level
+ 3.630 MeV Level
+ 3.710 MeV Level
+ 3.750 MeV Level
+ 3.790 MeV Level
+ 3.860 MeV Level

θ_{cm}	$d\sigma/d\omega$	Δ (%)	
deg.	mb/str	+	−
33.86	30.76	14.1	14.1
49.37	30.89	13.5	13.5
57.06	28.42	16.7	16.7
72.38	32.03	18.5	18.5
97.54	21.33	17.1	17.1
104.99	23.39	16.7	16.7
112.41	22.69	18.7	18.7
123.68	23.68	16.9	16.9
130.96	23.67	20.1	20.1
138.24	22.74	16.8	16.8

Avg. $d\sigma/d\omega$ = 25.34 mb/str ± 13.6 %
$\int(d\sigma/d\omega)d\omega$ = 318.41 mb ± 13.6 %

$E_n = 5.23 \pm 0.05$ MeV
(n,n′) to: 0.983 MeV Level

θ_{cm}	$d\sigma/d\omega$	Δ (%)	
deg.	mb/str	+	−
78.81	8.44	24.1	19.6
86.33	9.13	17.6	26.6

$\int(d\sigma/d\omega)d\omega$ = 120.00mb ± 18.0 %

Legendre Fit, Order = 0

k	a_k	Δ(%)
0	17.66521	13.7

$E_n = 5.23 \pm 0.05$ MeV
(n,n′) to: 2.295 MeV Level

θ_{cm}	$d\sigma/d\omega$	Δ (%)	
deg.	mb/str	+	−
71.52	5.45	23.1	23.1

Avg. $d\sigma/d\omega$ = 5.45mb/str ± 24.2 %
$\int(d\sigma/d\omega)d\omega$ = 68.42mb ± 24.2 %

$E_n = 5.23 \pm 0.05$ MeV
(n,n′) to: 2.295 MeV Level
+ 2.420 MeV Level

θ_{cm}	$d\sigma/d\omega$	Δ (%)	
deg.	mb/str	+	−
71.54	12.09	20.1	16.3
79.11	11.90	17.3	17.5
86.63	9.19	25.2	20.2

Avg. $d\sigma/d\omega$ = 11.25mb/str ± 13.4 %
$\int(d\sigma/d\omega)d\omega$ = 141.32mb ± 13.4 %

$E_n = 5.23 \pm 0.05$ MeV
(n,n′) to: 2.420 MeV Level

θ_{cm} deg.	$d\sigma/d\omega$ mb/str	△ (%) +	−
71.56	6.68	26.2	26.2

Avg. $d\sigma/d\omega$ = 6.68 mb/str ± 27.1 %
$\int(d\sigma/d\omega)d\omega$ = 83.97 mb ± 27.1 %

$E_n = 5.23 \pm 0.05$ MeV
(n,n′) to: 3.224 MeV Level
+ 3.240 MeV Level

θ_{cm} deg.	$d\sigma/d\omega$ mb/str	△ (%) +	−
79.43	8.83	21.0	21.0
86.97	8.01	26.9	26.9

Avg. $d\sigma/d\omega$ = 8.49 mb/str ± 18.5 %
$\int(d\sigma/d\omega)d\omega$ = 106.67 mb ± 18.5 %

$E_n = 5.23 \pm 0.05$ MeV
(n,n′) to: 3.224 MeV Level
+ 3.240 MeV Level
+ 3.340 MeV Level

θ_{cm} deg.	$d\sigma/d\omega$ mb/str	△ (%) +	−
71.85	10.21	22.6	22.6

Avg. $d\sigma/d\omega$ = 10.21 mb/str ± 23.6 %
$\int(d\sigma/d\omega)d\omega$ = 128.36 mb ± 23.6 %

$E_n = 5.23 \pm 0.05$ MeV
(n,n′) to: 3.224 MeV Level
+ 3.240 MeV Level
+ 3.340 MeV Level
+ 3.360 MeV Level
+ 3.380 MeV Level

θ_{cm} deg.	$d\sigma/d\omega$ mb/str	△ (%) +	−
71.89	21.08	14.0	15.6
79.48	21.07	12.9	17.5
87.02	20.46	13.4	20.0

Avg. $d\sigma/d\omega$ = 20.79 mb/str ± 12.3 %
$\int(d\sigma/d\omega)d\omega$ = 261.23 mb ± 12.3 %

$E_n = 5.23 \pm 0.05$ MeV
(n,n′) to: 3.340 MeV Level
+ 3.360 MeV Level
+ 3.380 MeV Level

θ_{cm} deg.	$d\sigma/d\omega$ mb/str	△ (%) +	−
79.52	10.84	25.7	25.7
87.05	11.19	22.4	22.4

Avg. $d\sigma/d\omega$ = 11.03 mb/str ± 18.8 %
$\int(d\sigma/d\omega)d\omega$ = 138.63 mb ± 18.8 %

$E_n = 5.23 \pm 0.05$ MeV
(n,n′) to: 3.360 MeV Level
+ 3.380 MeV Level

θ_{cm} deg.	$d\sigma/d\omega$ mb/str	△ (%) +	−
71.94	9.23	25.6	25.6

Avg. $d\sigma/d\omega$ = 9.23 mb/str ± 26.6 %
$\int(d\sigma/d\omega)d\omega$ = 115.94 mb ± 26.6 %

$E_n = 5.50 \pm 0.05$ MeV
(n,n′) to: 0.983 MeV Level

θ_{cm} deg.	$d\sigma/d\omega$ mb/str	△ (%) +	−
48.48	10.39	19.6	16.4
56.09	10.07	29.0	21.4
63.68	6.70	34.7	25.2

$\int(d\sigma/d\omega)d\omega = 110.00\,\text{mb} \pm 19.0\ \%$

Legendre Fit, Order = 0

k	a_k	△(%)
0	16.69496	12.2

$E_n = 5.50 \pm 0.05$ MeV
(n,n′) to: 2.295 MeV Level
+ 2.420 MeV Level

θ_{cm} deg.	$d\sigma/d\omega$ mb/str	△ (%) +	−
48.69	10.38	25.3	14.8
56.32	11.10	27.0	21.8
63.95	8.94	26.5	34.0

Avg. $d\sigma/d\omega = 10.21\,\text{mb/str} \pm 13.5\%$
$\int(d\sigma/d\omega)d\omega = 128.34\,\text{mb} \pm 13.5\ \%$

$E_n = 5.50 \pm 0.05$ MeV
(n,n′) to: 3.224 MeV Level
+ 3.240 MeV Level
+ 3.340 MeV Level
+ 3.360 MeV Level
+ 3.380 MeV Level

θ_{cm} deg.	$d\sigma/d\omega$ mb/str	△ (%) +	−
48.94	22.09	16.2	16.9
56.59	19.36	14.8	17.2
64.23	15.26	21.0	20.2

Avg. $d\sigma/d\omega = 18.62\,\text{mb/str} \pm 13.5\%$
$\int(d\sigma/d\omega)d\omega = 234.04\,\text{mb} \pm 13.5\ \%$

$E_n = 6.44 \pm 0.07$ MeV
Elastic Scattering

θ_{cm} deg.	$d\sigma/d\omega$ mb/str	△ (%) +	−
15.32	1866.04	4.0	6.2
22.96	1252.84	4.6	5.7
28.05	997.49	4.1	5.5
35.69	582.56	4.8	6.5
43.31	289.57	5.8	5.4
48.39	190.85	6.0	5.8
55.99	69.11	7.9	7.9
63.57	17.45	18.7	12.5
71.13	3.49	55.7	36.9
78.67	3.69	41.5	32.1
86.20	9.59	18.4	19.3
93.70	19.34	11.5	10.0
101.18	24.63	12.5	9.9
108.65	27.41	9.7	7.3
120.55	25.70	11.7	9.2
127.96	19.12	14.5	11.6
135.36	16.34	14.4	11.5

$\int(d\sigma/d\omega)d\omega = 2036.46\text{mb} \pm 7.3\%$
Wick's Limit = $2081.66\text{mb} \pm 7.4\%$
$\sigma_T = 3.32\text{b} \pm 1.2\%$

Legendre Fit, Order = 8

k	a_k	△(%)
0	324.11304	2.0
1	256.94751	2.3
2	199.12033	2.5
3	138.26901	2.9
4	75.73734	4.2
5	34.11031	7.2
6	14.19009	12.1
7	4.65857	22.8
8	1.05620	60.5

$E_n = 6.44 \pm 0.07$ MeV
(n,n′) to: 0.983 MeV Level

θ_{cm} deg.	$d\sigma/d\omega$ mb/str	△ (%) +	△ (%) −
35.75	15.55	19.3	25.5
43.38	12.00	30.6	22.9
48.46	12.46	17.6	18.0
56.07	9.25	19.5	16.7
63.66	7.59	16.4	18.0
71.23	6.75	16.6	15.9
78.77	5.59	11.4	11.0
86.30	5.06	14.8	18.0
93.80	6.12	17.7	11.5
101.28	7.38	20.5	18.0
108.75	7.84	13.8	16.6
120.64	9.09	19.6	18.0
128.04	8.84	14.8	16.2
135.43	11.40	16.4	15.3

$\int(d\sigma/d\omega)d\omega = 116.71$ mb $\pm$ 8.9 %

Legendre Fit, Order = 2

k	a_k	△(%)
0	18.57539	5.5
1	0.16166	383.0
2	2.94538	17.7

$E_n = 6.44 \pm 0.07$ MeV
(n,n′) to: 2.295 MeV Level
+ 2.420 MeV Level

θ_{cm} deg.	$d\sigma/d\omega$ mb/str	△ (%) +	△ (%) −
35.87	10.21	29.6	25.4
43.53	10.99	26.0	21.9
48.62	7.83	21.1	22.9
56.24	8.00	14.4	22.3
63.85	5.84	13.5	13.7
71.43	7.24	20.8	20.5
78.97	6.26	19.0	18.5
86.51	5.86	25.4	17.7
94.01	7.95	16.0	17.9
101.49	7.36	19.3	22.1
108.95	7.23	21.2	19.8
120.82	7.38	14.1	16.0
128.22	8.38	12.6	21.7
135.58	5.80	12.1	25.6

Avg. $d\sigma/d\omega =$ 6.73mb/str $\pm$ 9.4 %
$\int(d\sigma/d\omega)d\omega =$ 84.60mb $\pm$ 9.4 %

$E_n = 6.44 \pm 0.07$ MeV
(n,n′) to: 3.224 MeV Level
+ 3.240 MeV Level
+ 3.340 MeV Level
+ 3.360 MeV Level
+ 3.380 MeV Level

θ_{cm} deg.	$d\sigma/d\omega$ mb/str	△ (%) +	△ (%) −
36.00	11.92	19.2	17.8
43.67	13.24	19.3	25.6
48.78	15.58	16.0	28.2
56.43	15.19	9.6	24.2
64.04	12.19	8.9	22.0
71.63	13.56	9.5	23.8
79.20	12.50	11.1	24.3
86.73	13.06	8.6	24.9
94.24	13.91	9.3	24.1
101.71	12.14	14.8	22.4
109.16	12.12	10.3	26.1
121.01	13.43	11.8	22.8
128.39	12.30	13.2	27.5
135.74	12.98	11.5	24.1

Avg. $d\sigma/d\omega$ = 12.49 mb/str ± 9.2 %
$\int(d\sigma/d\omega)d\omega$ = 156.91 mb ± 9.2 %

$E_n = 7.03 \pm 0.06$ MeV
(n,n′) to: 0.983 MeV Level

θ_{cm} deg.	$d\sigma/d\omega$ mb/str	△ (%) +	△ (%) −
71.22	5.00	15.3	13.8
78.76	3.93	9.5	25.6
86.29	4.77	12.9	17.1

$\int(d\sigma/d\omega)d\omega$ = 90.00 mb ± 13.0 %

Legendre Fit, Order = 0

k	a_k	△(%)
0	9.13271	8.6

$E_n = 7.03 \pm 0.06$ MeV
(n,n′) to: 2.295 MeV Level
+ 2.420 MeV Level

θ_{cm} deg.	$d\sigma/d\omega$ mb/str	△ (%) +	△ (%) −
71.39	4.40	18.7	15.2
78.94	4.58	13.5	22.2
86.47	4.69	13.7	26.0

Avg. $d\sigma/d\omega$ = 4.52mb/str ± 14.7 %
$\int(d\sigma/d\omega)d\omega$ = 56.74mb ± 14.7 %

$E_n = 7.03 \pm 0.06$ MeV
(n,n′) to: 3.224 MeV Level
+ 3.240 MeV Level
+ 3.340 MeV Level
+ 3.360 MeV Level
+ 3.380 MeV Level

θ_{cm} deg.	$d\sigma/d\omega$ mb/str	△ (%) +	△ (%) −
71.57	9.54	8.3	24.5
79.13	9.36	12.2	25.4
86.66	8.95	10.7	25.3

Avg. $d\sigma/d\omega$ = 9.06mb/str ± 11.8 %
$\int(d\sigma/d\omega)d\omega$ = 113.85mb ± 11.8 %

$E_n = 7.54 \pm 0.06$ MeV
Elastic Scattering

θ_{cm}	$d\sigma/d\omega$	Δ (%)	
deg.	mb/str	+	−
15.32	1785.59	5.2	6.0
22.96	1221.89	4.7	6.1
28.06	860.07	6.3	5.0
35.69	467.44	5.4	4.6
43.31	198.50	7.0	6.4
48.39	101.20	9.7	7.5
55.98	27.04	11.8	10.5
63.57	8.77	17.3	22.2
71.13	2.90	47.4	41.0
78.67	4.12	23.4	24.8
86.20	6.96	19.4	20.5
93.70	12.10	16.5	14.8
101.18	19.41	10.4	14.8
108.64	22.46	11.3	15.0
120.54	20.13	8.4	12.9
127.96	14.76	13.3	15.2
135.36	11.69	9.7	12.8

$\int(d\sigma/d\omega)d\omega = 1767.02$ mb $\pm$ 7.4 %
Wick's Limit = 2207.97 mb $\pm$ 8.1 %
$\sigma_T =$ 3.16 b $\pm$ 2.0 %

Legendre Fit, Order = 9

k	a_k	Δ(%)
0	281.23096	2.3
1	230.97852	2.6
2	186.83694	2.8
3	138.37357	3.1
4	84.72981	4.2
5	45.01607	6.2
6	21.89610	9.5
7	8.02285	17.3
8	1.74674	49.6
9	0.04707	995.2

$E_n = 7.54 \pm 0.06$ MeV
(n,n′) to: 0.983 MeV Level

θ_{cm}	$d\sigma/d\omega$	Δ (%)	
deg.	mb/str	+	−
35.74	13.85	23.1	28.2
43.37	8.51	23.8	41.5
48.45	8.08	21.5	32.5
56.05	6.32	13.5	14.8
63.64	4.45	16.5	16.1
71.21	4.55	12.6	15.8
78.76	3.03	30.8	14.4
86.28	2.67	36.8	20.7
93.79	2.66	29.5	31.9
101.26	4.99	22.7	35.8
108.73	6.70	18.8	21.2
120.62	6.21	17.9	20.0
128.03	5.84	15.4	18.2
135.42	7.14	15.3	14.4

$\int(d\sigma/d\omega)d\omega = 74.97$mb $\pm$ 9.1 %

Legendre Fit, Order = 2

k	a_k	Δ(%)
0	11.93194	5.8
1	0.28866	153.7
2	2.22458	18.2

$E_n = 7.54 \pm 0.06$ MeV
(n,n′) to: 2.295 MeV Level
+ 2.420 MeV Level

θ_{cm} deg.	$d\sigma/d\omega$ mb/str	△ (%) +	△ (%) −
35.84	3.06	17.8	17.8
43.49	4.94	19.3	30.1
48.58	4.23	29.2	30.8
56.19	3.60	58.7	35.0
63.79	3.57	28.1	22.1
71.36	3.13	18.7	21.0
78.92	2.53	38.1	18.4
86.45	3.56	21.2	19.5
93.95	4.08	36.1	19.0
101.43	3.28	27.7	40.4
108.89	4.61	20.1	24.6
120.76	4.00	30.4	32.6
128.16	2.68	20.4	22.0
135.54	3.19	27.8	24.0

Avg. $d\sigma/d\omega$ = 3.34 mb/str ± 10.2 %
$\int(d\sigma/d\omega)d\omega$ = 41.92 mb ± 10.2 %

$E_n = 7.54 \pm 0.06$ MeV
(n,n′) to: 3.224 MeV Level
+ 3.240 MeV Level
+ 3.340 MeV Level
+ 3.360 MeV Level
+ 3.380 MeV Level

θ_{cm} deg.	$d\sigma/d\omega$ mb/str	△ (%) +	△ (%) −
35.93	6.32	28.9	28.9
48.69	9.62	12.9	38.1
56.32	8.02	21.5	27.9
63.93	7.98	11.2	31.3
71.52	7.29	15.8	20.1
79.07	7.38	17.2	26.6
86.61	6.55	15.6	25.4
94.11	6.16	20.1	20.1
101.59	6.16	23.0	29.3
109.04	6.95	12.9	30.1
120.90	8.35	11.4	24.2
128.29	6.20	18.3	20.7
135.66	6.46	10.8	26.1

Avg. $d\sigma/d\omega$ = 6.67 mb/str ± 9.7 %
$\int(d\sigma/d\omega)d\omega$ = 83.78 mb ± 9.7 %

$E_n = 8.04 \pm 0.05$ MeV
(n,n′) to: 0.983 MeV Level

θ_{cm} deg.	$d\sigma/d\omega$ mb/str	△ (%) +	△ (%) −
71.20	4.14	25.5	21.0
78.75	4.31	19.0	21.1
86.28	3.88	19.4	14.1

$\int(d\sigma/d\omega)d\omega$ = 80.00 mb ± 14.0 %

Legendre Fit, Order = 0

k	a_k	△(%)
0	8.07117	10.5

$E_n = 8.04 \pm 0.05$ MeV
(n,n′) to: 2.295 MeV Level
+ 2.420 MeV Level

θ_{cm} deg.	$d\sigma/d\omega$ mb/str	△ (%) +	△ (%) −
71.34	2.96	33.3	24.7
78.90	3.98	28.7	26.1
86.42	2.78	29.8	20.7

Avg. $d\sigma/d\omega$ = 3.16 mb/str ± 18.7 %
$\int(d\sigma/d\omega)d\omega$ = 39.71 mb ± 18.7 %

$E_n = 8.04 \pm 0.05$ MeV
(n,n′) to: 3.224 MeV Level
+ 3.240 MeV Level
+ 3.340 MeV Level
+ 3.360 MeV Level
+ 3.380 MeV Level

θ_{cm} deg.	$d\sigma/d\omega$ mb/str	△ (%) +	△ (%) −
71.48	5.36	20.1	28.6
79.04	6.80	20.6	20.5
86.57	6.92	13.6	25.6

Avg. $d\sigma/d\omega$ = 6.09 mb/str ± 14.7 %
$\int(d\sigma/d\omega)d\omega$ = 76.50 mb ± 14.7 %

$E_n = 8.56 \pm 0.05$ MeV
Elastic Scattering

θ_{cm} deg.	$d\sigma/d\omega$ mb/str	△ (%) +	△ (%) −
15.31	1688.05	5.2	4.3
22.96	1177.64	5.0	5.1
28.06	664.63	5.8	4.2
35.69	319.38	6.0	7.1
43.31	120.38	8.4	10.1
48.39	78.84	6.1	9.1
55.99	25.23	9.6	15.4
63.57	10.19	16.6	18.1
71.13	7.30	23.9	18.8
78.67	5.83	31.0	15.7
86.20	5.41	30.6	18.7
93.70	11.46	9.0	10.2
93.70	10.79	13.2	18.4
101.18	16.88	7.1	11.6
101.18	17.11	5.7	14.2
108.64	21.05	10.9	6.9
108.65	22.18	11.9	7.8
120.54	24.14	7.7	11.5
127.96	15.29	14.6	14.6
135.36	9.47	16.6	22.6

$\int(d\sigma/d\omega)d\omega = 1546.67$ mb ± 7.4 %
Wick's Limit = 2274.33 mb ± 8.1 %
$\sigma_T = 3.01$ b ± 2.0 %

Legendre Fit, Order = 10

k	a_k	△(%)
0	246.16020	2.2
1	202.50555	2.5
2	167.16641	2.7
3	130.40965	3.0
4	86.02414	3.8
5	52.63818	5.3
6	31.67497	7.1
7	15.67540	11.1
8	6.79768	17.3
9	2.88917	24.9
10	0.85988	43.9

$E_n = 8.56 \pm 0.05$ MeV
(n,n′) to: 0.983 MeV Level

θ_{cm} deg.	$d\sigma/d\omega$ mb/str	△ (%) +	△ (%) −
35.73	8.14	19.2	36.8
43.36	7.39	36.7	27.7
48.44	8.57	12.9	21.6
56.05	6.87	8.8	19.2
63.63	4.85	14.4	15.7
71.19	3.69	23.5	33.7
78.74	3.97	19.2	28.4
86.27	4.19	21.3	21.4
93.77	5.41	18.8	17.6
93.77	4.08	9.5	26.5
101.25	3.76	44.9	30.7
101.26	5.13	15.4	17.5
108.71	3.51	41.1	24.2
108.71	4.39	11.9	17.0
120.61	7.34	13.5	17.8
128.02	8.04	13.7	11.4
135.41	6.80	19.7	20.1

$\int(d\sigma/d\omega)d\omega = 78.98$mb ± 8.8 %

Legendre Fit, Order = 2

k	a_k	△(%)
0	12.57071	5.4
1	−0.02012	2004.6
2	1.69351	21.3

$E_n = 8.56 \pm 0.05$ MeV
(n,n′) to: 2.295 MeV Level
+ 2.420 MeV Level

θ_{cm}	$d\sigma/d\omega$	△ (%)	
deg.	mb/str	+	−
43.46	4.78	31.0	24.5
48.54	2.48	20.5	40.1
56.16	2.69	34.8	28.5
63.76	2.38	25.8	32.2
78.88	1.83	47.8	36.8
93.91	2.50	41.1	23.3
93.91	1.85	49.0	32.9
101.39	1.66	86.5	37.5
108.85	2.47	30.7	24.2
128.13	2.85	43.3	28.3

Avg. $d\sigma/d\omega$ = 2.50 mb/str ± 12.7 %
$\int(d\sigma/d\omega)d\omega$ = 31.45 mb ± 12.7 %

$E_n = 8.56 \pm 0.05$ MeV
(n,n′) to: 3.224 MeV Level
+ 3.240 MeV Level
+ 3.340 MeV Level
+ 3.360 MeV Level
+ 3.380 MeV Level

θ_{cm}	$d\sigma/d\omega$	△ (%)	
deg.	mb/str	+	−
35.89	8.25	15.0	43.4
43.54	6.96	21.6	23.3
48.64	6.46	16.8	33.8
56.26	6.52	10.0	30.3
63.87	6.06	20.8	32.7
71.45	4.34	35.5	23.3
79.00	4.45	21.0	32.8
86.53	4.96	14.2	24.4
94.04	4.80	19.0	35.9
94.04	5.01	21.9	34.3
101.51	5.07	24.9	37.3
101.52	4.95	17.1	29.4
108.97	4.75	27.0	30.1
108.97	4.85	14.2	32.2
120.84	4.70	28.8	26.1
128.23	4.77	23.1	28.4
135.60	3.62	32.0	21.6

Avg. $d\sigma/d\omega$ = 4.90 mb/str ± 10.1 %
$\int(d\sigma/d\omega)d\omega$ = 61.54 mb ± 10.1 %

ORNL-4810
UC-79d - Physics

INTERNAL DISTRIBUTION

1-3. Central Research Library
4. ORNL - Y-12 Technical Library Document Reference Section
5-24. Laboratory Records Department
25. Laboratory Records, ORNL R.C.
26-28. L. S. Abbott
29. R. G. Alsmiller, Jr.
30. C. E. Clifford
31. F. L. Culler
32. J. K. Dickens
33. C. Y. Fu
34. W. O. Harms
35. R. F. Hibbs
36-145. W. E. Kinney
146. T. A. Love
147-148. F. C. Maienschein
149. G. L. Morgan
150. F. R. Mynatt
151. E. M. Oblow
152. R. W. Peelle
153. S. K. Penny
154-168. F. G. Perey
169. R. W. Roussin
170. M. J. Skinner
171. A. M. Weinberg
172. A. Zucker
173. H. Feshbach (Consultant)
174. P. F. Fox (Consultant)
175. C. R. Mehl (Consultant)
176. H. T. Motz (Consultant)

EXTERNAL DISTRIBUTION

177-178. USAEC Division of Reactor Research and Development, Washington, D.C. 20545
179. USAEC-RRD Senior Site Representative, ORNL
180. Research and Technical Support Division, AEC, ORO
181-411. Given distribution as shown in TID-4500 under UC-79d, Liquid Metal Fast Breeder Reactors (Physics)